Physics of Plasmas

On the role of fluctuations, cathode placement, and collisions on the transport of electrons in the near-field of Hall thrusters

Cite as: Phys. Plasmas **17**, 093501 (2010); https://doi.org/10.1063/1.3479827
Submitted: 05 April 2010 . Accepted: 26 July 2010 . Published Online: 02 September 2010

A. W. Smith, and M. A. Cappelli

On the role of fluctuations, cathode placement, and collisions on the transport of electrons in the near-field of Hall thrusters

A. W. Smith[1,a)] and M. A. Cappelli[2]
[1]*Department of Mechanical Engineering, Stanford University, Bldg. 520, 521E, Stanford, California 94305-3032, USA*
[2]*Department of Mechanical Engineering, Stanford University, Bldg. 520, 520D, Stanford, California 94305-3032, USA*

(Received 5 April 2010; accepted 26 July 2010; published online 2 September 2010)

The performance of Hall thrusters can be highly sensitive to the position and operational parameters of the external cathode, hinting that the electron transport in the near-field is strongly dependent on the emitted electrons' initial properties. In addition, the plasma plumes of Hall discharges often exhibit fluctuations which are expected to alter electron trajectories. By implementing recent near-field plasma potential measurements made on a low-power Hall thruster in 3D electron-trajectory simulations, it is shown that electron transport from the external cathode to the thruster channel is strongly sensitive to cathode parameters including position, orientation, and electron emission divergence. Periodic, low-frequency (i.e., 25 kHz) plasma potential fluctuations reduce electron transport to the channel of the thruster by more than 65% compared to the transport achieved with static 3D fields and substantially homogenize the electron density distribution. Additional gas-phase collisions are found to have only marginal effects, even when prescribed to occur at exaggerated rates (reaching 10 MHz). The three-dimensionality of the $\boldsymbol{E}$ and $\boldsymbol{B}$ fields, together with electron-wall collisions, appear to be important drivers of cross-field transport in this region of the discharge, yielding sufficient levels of electron transport to the channel without invoking plasma turbulence. © *2010 American Institute of Physics*. [doi:10.1063/1.3479827]

I. MOTIVATION AND BACKGROUND

Hall-effect thrusters have been used as high-efficiency electric propulsion devices for nearly 50 years.[1,2] Though a variety of geometries have been developed, annular designs are one of the most common. Annular Hall thrusters, such as that schematically illustrated in Fig. 1, are comprised of an annular channel (at the base of which the anode is generally found) and a series of electromagnets that produce a predominantly radial magnetic field near the channel exit. The magnitude of the imposed magnetic field is set such that electrons near the channel exit are confined in closed, azimuthal $\boldsymbol{E}\times\boldsymbol{B}$ drifts, while the massive ions are essentially nonmagnetized. Due to the reduced axial mobility of electrons, the strong field that ensues accelerates ions to velocities of the order of 10 km/s.[3] A cathode, often located outside the annular channel, injects electrons that serve both to neutralize the ion beam and to sustain the discharge. In a typical annular $\boldsymbol{E}\times\boldsymbol{B}$ Hall thruster, approximately 10% of the electron current emitted by the cathode migrates into the thruster to service the discharge, while the remainder serves to neutralize the ion beam.[4]

The performance of Hall thrusters and other similar discharges is frequently sensitive to cathode parameters including position, orientation, and operational settings.[5–8] In the near-field region, defined to lie between the exit of the channel and the cathode, a Bohm model for the electron mobility is frequently assumed,[9,10] despite the lack of strong evidence linking plasma fluctuations and transport in this region. Recent kinetic studies indicate that electron transport to the channel from the cathode is strongly dependent on collisions with the front-face of the thruster.[11] Given the geometry of the magnetic field lines in the vicinity of the cathode (see Fig. 2), it is clear that altering the position of the cathode will change the initial magnetic field lines electrons travel on and modify the locations of wall-collision events. This change in trajectory may lead to fewer electrons reaching the channel of the thruster and therefore a correlated change in the operational performance of the main discharge. Furthermore, the plasma potential in the near-field of Hall thrusters sometimes exhibits strong fluctuations, including low-frequency (25 kHz) helical fluctuations,[12] and these fluctuations likely play a role in the electron transport between the cathode and the thruster channel.

Among the most frequently utilized tools for simulating the discharge and near-field region of Hall thrusters are quasineutral hybrid-particle-in-cell (PIC) methods in which the electrons are modeled as a fluid and the ions and neutrals are treated kinetically as particles.[13–17] Such simulations are generally 2D [either radial-axial, r-z,[13] or axial-azimuthal, z-θ (Ref. 17)] and proceed self-consistently with the ion movement influenced by the electric potential, derived from an equation for the average electron velocity, assuming some constitutive relation for the cross-field electron current. In addition to the limitations imposed by 2D simulations, those models that do not resolve the azimuthal dimension (along the direction of electron drift) must rely on the use of *ad hoc* transport descriptions such as an electron mobility that scales as $|\boldsymbol{B}|^{-1}$, in accordance with the model of Bohm,[18] or equiva-

[a)]Electronic mail: awsmith@stanford.edu.

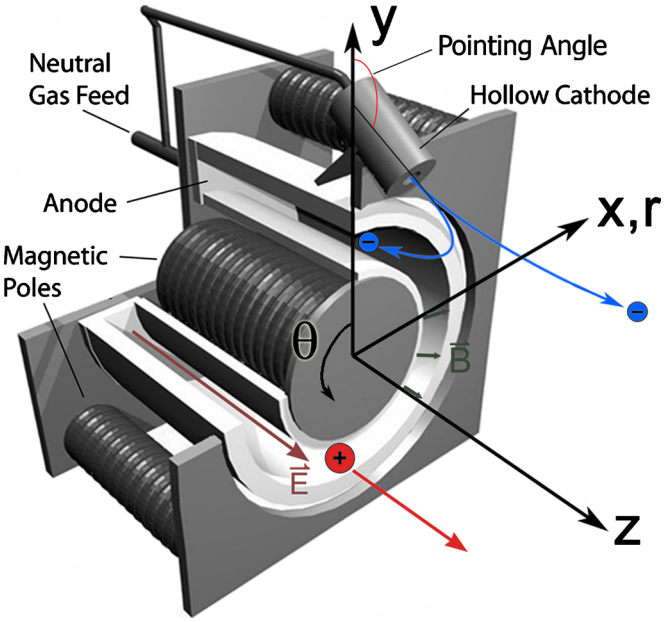

FIG. 1. (Color online) Schematic of a typical annular Hall thruster with major components labeled.

lently, a constant effective Hall parameter, $\omega_c \tau_{eff}$. Here, ω_c is the electron-cyclotron frequency and t_{eff} is the effective time between scattering events. This Hall parameter is often used as a tuning parameter, exaggerated to enhance the cross-field electron mobility to achieve good agreement between simulations and experiments. Models that do resolve the motion in the azimuthal direction attempt to drive electron current via correlated fluctuations in plasma density and plasma potential, loosely described as plasma turbulence[19] when the propagation direction of these fluctuations is independent of position and the fluctuations span a wide range of spatial scales. The goal of our research is to better understand significance of other potential transport mechanisms for the near-field region of these discharges, such as electron-wall collisions, when there are also strong spatial variations in the electric and magnetic fields.

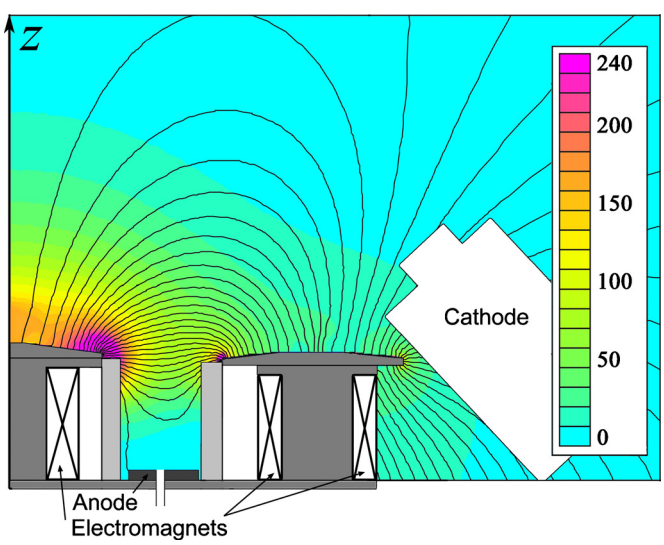

FIG. 2. (Color online) Cross section of a typical annular Hall thruster with superimposed magnetic field lines. The shading denotes the magnetic field strength in gauss.

This paper is an extension of previous research[11] which seeks to understand the near-field electron transport through detailed electron trajectory simulations. In our earlier work, we used an estimated, axisymmetric field distribution in the simulations as no measurements were available at that time. In the current work, the results of 3D, time-resolved plasma potential measurements[12] made on a low-power (200 W, 250 V anode potential) Hall thruster are incorporated into our simulations. Also, the spatial position and orientation of a simulated electron source (cathode) are varied and the resulting electron current distributions (i.e., channel/beam current ratios) and diffusion rates are compared. In some simulations, additional gas-phase collisions are introduced at expected and exaggerated rates; in others the effects of axisymmetric fields are investigated.

II. SIMULATION

Our current study focuses on computing discrete particle trajectories of electrons in the near-field of a typical low-power annular geometry Hall thruster. The time-fluctuating electric field used to move the electrons is derived from emissive probe measurements made on a low-power Hall thruster.[12] In principle, full 3D PIC simulations could be carried out with the simultaneous self-consistent tracking of a large number of superparticles (electrons and ions); however, such simulations are still intractable for the full geometry of a typical Hall thruster. Instead, we prescribe the electric field distribution (spatially and temporally), allowing for a relatively smaller number of particles to be considered.

Time-synchronized plasma potential measurements obtained within a large portion of the near-field[12] are used to motivate the plasma potential distribution considered in this study. The measured plasma potential distribution was linearly interpolated to a 2 mm mesh, then smoothed by taking the average value of seven neighboring points (the central point for which the smoothed value is being calculated, and the two bracketing points in x, y, and z). The time-average of this potential is shown in Fig. 3(a). While this method introduces uncertainty in the distribution, it is within the experimental uncertainty ($\pm > 17\%$). The plasma potential at the far-field simulation boundaries was prescribed as 0 V; the potential was linearly interpolated between this value and that at the experimental measurement limits. The same interpolation and smoothing methods were applied for the plasma potential fluctuation amplitude distribution, shown in Fig. 3(b). A uniform sheath of thickness 1 mm (approximately the Debye length assuming $n_e \sim 10^9$ cm^{-3} and $T_e \sim 5$ eV immediately adjacent to the thruster face) and potential drop 15 V was applied on all thruster surfaces as done in the previous work.[11] This value is an estimate motivated by the simplified analysis presented by Bittencourt,[20] which gives the wall potential relative to the bulk plasma (the sheath potential drop) as $\Delta\phi = -kT \ln(m_i/m_e)/(4e)$ where k is Boltzmann's constant, T is the effective temperature of the plasma (assuming the electrons and ion are in thermodynamic equilibrium at the same temperature, T), e is the fundamental charge, and m_i

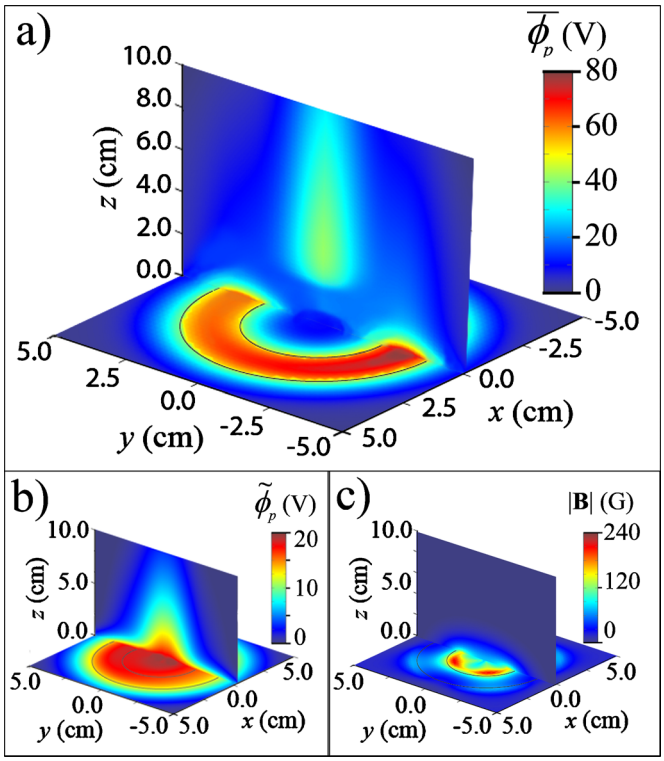

FIG. 3. (Color online) Field distributions utilized in the simulations: (a) mean plasma potential, $\overline{\phi_p}(x,y,z,t)$ (in volts), (b) plasma potential fluctuation magnitude, $\tilde{\phi}_p(x,y,z,t)$ (in volts), and (c) magnetic field magnitude, $|\boldsymbol{B}|$ (in gauss). The azimuthal variation in the plasma potential and magnetic field strength are evident; the fluctuation magnitude also varies azimuthally, though to a lesser extent.

and m_e are the ion and electron masses, respectively. For a xenon plasma, $\ln(m_i/m_e)\sim 12.4$. The 15 V sheath potential is obtained by assuming that the equilibrium temperature in the near-field is of the order of 5 eV, giving $\Delta\phi=15.5$ V. The fields were discretized to 2 mm grids, spanning $x,y=\pm 300$ mm and 0 mm$\leq z\leq 300$ mm (i.e., the exit plane to 300 mm downstream of the exit plane).

The nominal simulation, considered 3D fields with a 25 kHz helical plasma potential fluctuation observed in time-synchronized measurements.[12] The fluctuating potential is represented by

$$\phi_p(x,y,z,t) = \overline{\phi_p}(x,y,z,t) + A\tilde{\phi}_p(x,y,z,t) \times \sin(2\pi f[t - t_{\text{lag}}(x,y,z)]), \quad (1)$$

where $\overline{\phi_p}(x,y,z,t)$ is the mean plasma potential [Fig. 3(a)], $\tilde{\phi}_p(x,y,z,t)$ is the amplitude of the plasma potential fluctuation [Fig. 3(b)], A is an adjustable amplitude coefficient ($A=1$ in the nominal simulation, closely approximating what is seen experimentally), $f=25$ kHz, and

$$t_{\text{lag}}(x,y,z) = \frac{\theta}{2\pi f} + \frac{z}{bf}. \quad (2)$$

Here, θ is the azimuthal position (see Fig. 1) and b is the axial spacing of the helical waves (estimated at 5 cm from the experimental data). The fluctuation represents a helical wave with an azimuthal propagation in the $-\boldsymbol{E}\times\boldsymbol{B}$ direction, as observed in the experiments.

The near-field magnetic field distribution used in the simulations is expected to be dominated by the externally applied field of the thruster's magnetic circuit.[21] Induced magnetic fields (steady or fluctuating) generated by currents within the plasma are neglected. We use finite element method magnetics,[22] a finite element magnetic solver, to simulate the magnetic field distribution [see Fig. 3(c)]. The magnetic field for the thruster on which the plasma potential measurements were executed is unavailable, so a similar laboratory Hall discharge was used in the model. As a result, the plasma potential distributions shown in Figs. 3(a) and 3(b) have been scaled in space by the ratio of the mean channel radii of the two thrusters, an expansion of 28.7 mm/11.7 mm$\sim$2.45 times. The larger thruster had a discharge power and current of 350 W and 2.5 A, 1.75 and $\sim$3 times greater than the smaller discharge, respectively. The higher current was used to normalize the particle fluxes as described in Sec. III. The distribution is not axisymmetric due to the presence of the four discrete outer electromagnets (e.g., see Fig. 1) in the simulated thruster.

The particles are tracked using a fourth-order Runge–Kutta (RK4) integrator[23] for the equations of motion, as in the previous study. An adaptive time-step is utilized, with the local time-step selected to be 1% of the local cyclotron period. Electrons released from a point-source cathode are tracked until they exit the simulation domain, spanning $x,y=\pm 300$ mm and 0 mm$\leq z\leq 300$ mm (the exit plane is prescribed to be $z=0$, and the central axis is at $[x,y]=[0,0]$). The details of the electron launch are described in the previous work.[11] Unless otherwise noted, the cathode was located at $[x,y,z]=[0,78.4,22.0]$ mm (or $[r,z,\theta]=[78.4\text{ mm},22.0\text{ mm},0°]$), the same as the experimental position. The fluctuation period was divided into 100 equal segments (i.e., for the 25 kHz fluctuation implemented in this study, each segment spanned 400 ns), and 1% of the electrons (i.e., 1000 electrons in the current study) were released from the simulated cathode at the beginning of each time segment. The potential was continuously varied according to Eqs. (1) and (2) during the electrons' lifetimes. Once every virtual nanosecond, the position and velocity components of the particles are recorded. Postprocessing the data yields maps of the electron density, mean electron identity (i.e., channel-bound or plume-bound), and mean electron energy. In addition, wall-collision and domain-crossing locations are cataloged, allowing us to reconstruct the complete history for each electron.

Electrons colliding with thruster surfaces are assumed to be re-emitted with a random direction and a speed sampled from a 500 K Maxwellian speed distribution. Recombination events and other wall-collision physics are not considered in this study. In some simulations, we include additional gas-phase collisions at prescribed rates. During each of these events, electrons maintain their precollision energy, but their velocity is randomized.

An additional simulation considers the effects of field symmetry (in $\boldsymbol{E}$ and $\boldsymbol{B}$). The axisymmetric fields (not shown in Fig. 3) were obtained by azimuthally averaging the static plasma potential and magnetic field distributions shown in Fig. 3.

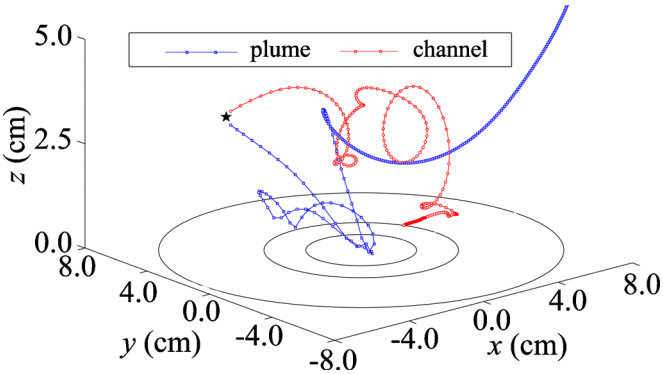

FIG. 4. (Color online) Representative electron trajectories observed in the 3D fluctuating simulation. The three ellipses represent the inner and outer channel boundaries and the thruster boundary. The location of the cathode is indicated by a star.

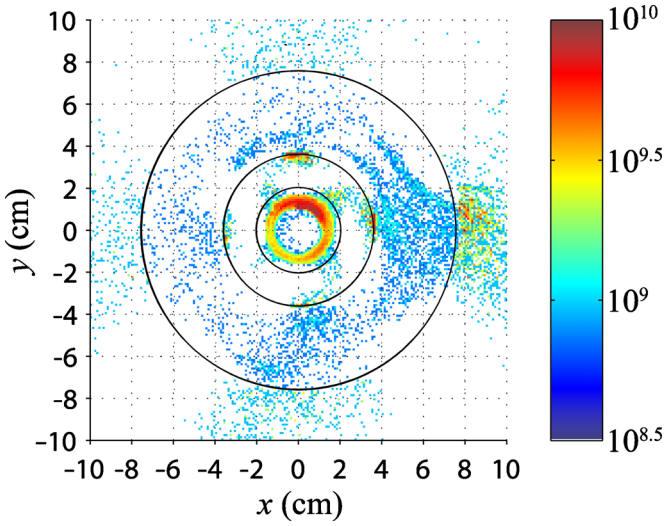

FIG. 5. (Color online) Flux ($\mathrm{mm}^{-2}\,\mathrm{s}^{-1}$) of wall-collision and electron domain-crossing events in the $z=0$ plane (i.e., the exit plane) plotted on a logarithmic scale. The channel boundaries and outer thruster boundary are indicated by circles The cathode was located at $[x,y,z]=[0.00,7.84,2.20]$ cm.

III. RESULTS

A. Nominal simulation

The "nominal" simulation considered 3D $\boldsymbol{E}$ and $\boldsymbol{B}$ distributions (shown in Fig. 3), with a helical plasma potential fluctuation [described by Eqs. (1) and (2)] which is inspired by experimental evidence of such a fluctuation.[12] A total of 10^4 electrons were launched in the simulation; a modest number due to the computational expense of continuously varying the plasma potential.

The fraction of electrons reaching the channel and plume was found to be 0.11 and 0.89, respectively, and the overall mean lifetime of electrons in the domain was 1.88 μs. Electrons that leave the domain at the channel (hereafter referred to as "channel-bound") tend to have significantly longer lifetimes (averaging 6.55 μs) than electrons which leave the domain elsewhere (hereafter referred to as "plume-bound"). Each channel-bound electron suffered an average of 32.7 wall collisions before reaching the channel, while plume-bound electrons averaged just 3.6 wall-collision events each. This result explains part of the lifetime discrepancy. The postcollision energy of the electrons is sampled from a 500 K Maxwellian distribution; in general collisions significantly reduce the electron energy (and speed). Two sample electron trajectories are plotted in Fig. 4. The location of the simulated cathode is indicated with a star and the channel boundaries and outer thruster boundary are illustrated as solid lines in the $z=0$ plane.

The distribution of wall collisions and electron domain-crossing events in the $z=0$ plane are shown in Fig. 5. To obtain the values in the figure, the fluxes observed in the simulation were normalized by the discharge current of the thruster (i.e., by the number of electrons emitted by the cathode in the *experiment* during the period of time spanned by the lifetime of the simulated electrons). Therefore, each simulated electron represents $\sim 10^8$ electrons.

The highest flux of wall-collision events occurs in a ring-shaped region over the inner pole of the thruster, where the flux exceeds 10^{10} $\mathrm{mm}^{-2}\,\mathrm{s}^{-1}$. A moderate flux density of wall collisions is observed on the outer annular pole piece of the thruster as well. Electrons reach the channel in a variety of regions, but the highest fluxes are observed near the outer channel boundary, primarily in the regions of lowest magnetic field strength between the outer magnetic poles (e.g., at $[x,y]\approx[0,4]$ cm), where the magnetic field strength is roughly 70% of that found nearest the electromagnets (for a given radial position). Many of the wall-collision locations are directly adjacent to the regions in which electrons reach the channel. Electrons colliding with the thruster are freed from their precollision magnetic field line; those colliding near the channels tend to diffuse toward the channel under the influence of the radial component of the electric field. Thus, near-wall transport[24] on the front-face of the thruster is partially responsible for allowing electrons to cross the magnetic field lines and reach the channel. Some of the electrons are also leaving the domain outside the thruster (e.g., near $[x,y]=[8,0]$ cm). One limitation of the model is that electrons leaving the domain are not permitted to return (as they would, for instance, on large gyroradii orbits). Different boundary conditions may be applied in future studies.

A spatial map of the electron density, n_e, is plotted on a logarithmic scale (with units of cm^{-3}) in Fig. 6(a). Figure 6(b) is a spatial map of the mean electron "identity." The identity of an electron is defined to equal 1 if it is channel-bound, whereas the identity of plume-bound electrons is defined to be 2. The mean electron energy, E_e, is illustrated in Fig. 6(c). The vertical axis of each stacked subfigure shows the midpoint of the axial range of the data in each slice. The true axial thickness of the planes is 1 cm. For example, the color plot at $z=1.5$ cm actually represents statistics gathered in 1 cm$\leq z<2$ cm. The channel and thruster boundaries are indicated in the $z=0.5$ cm planes by dark circles.

The spatial distribution of electrons [Fig. 6(a)] is moderately uniform over azimuthal position and is highest over the thruster, particularly over the central pole and channel where the density exceeds 10^{11} cm^{-3} (as before, the electron density was normalized using the thruster discharge current).

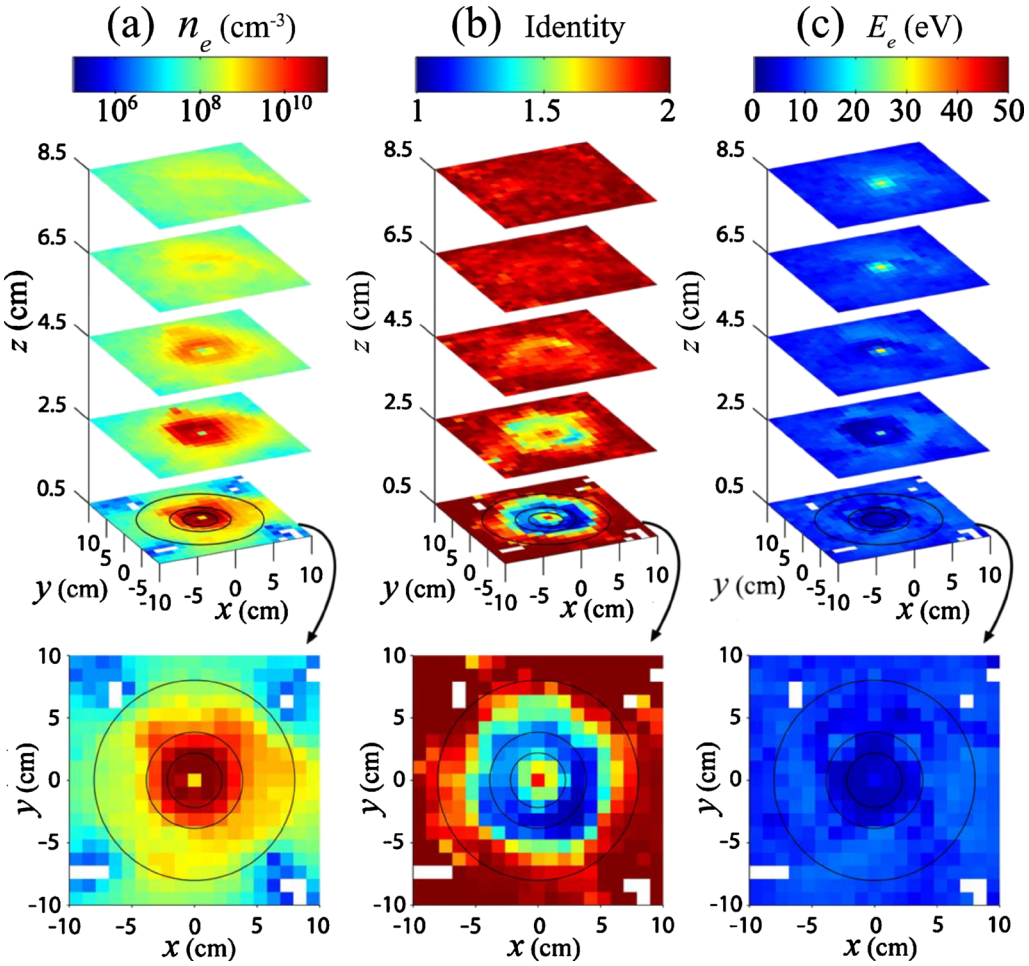

FIG. 6. (Color online) Simulated distributions of (a) electron density (in units of cm−3, on a logarithmic scale), (b) identity (1 is channel-bound, 2 is plume-bound), and (c) mean energy (eV) at several axial locations. The results are for the BHT-200 simulation with helical fluctuations in plasma potential.

In contrast, the density in the immediate vicinity of the central axis is two orders of magnitude lower. The reduced electron density along the central axis is in keeping with experimental microwave interferometry measurements.[25] In the $z=0.5$ cm plane, no electrons are found over the locations of the outer electromagnets where electrons tend to be mirrored by the converging $\boldsymbol{B}$-field; a similar, though less-prominent effect may also be responsible for reflecting electrons away from the central axis region. The presence of the cathode is evident as a small high density region near $[x,y,z]=[0,8,2.5]$ cm.

The spatial distribution of the mean electron identity [Fig. 6(b)] shows that the electrons near the exit plane within about $r\leq 5$ cm are channel-bound (i.e., have a mean identity close to 1), with the exception of the regions nearest the central axis (which are rich in plume-bound electrons). Channel-bound electrons are primarily found for $z\leq 4$ cm, though some are still present beyond $z=9$ cm, indicating that some electrons travel on long, arcing trajectories *en route* to the channel from the cathode. The central axis is likely rich in plume-bound electrons because the magnetic field lines are oriented axially here, providing electrons a path for exiting the domain.

The mean electron energy [Fig. 6(c)] is lower than that expected based on the plasma potential, except in the immediate vicinity of the central axis. The energy disparity is greatest where the electron population is dominated by channel-bound electrons [i.e., where the mean identity is close to unity, see Fig. 6(b)]. This is due to the fact that channel-bound electrons suffer frequent collisions in regions of high-plasma potential (such as near the channel boundaries, see Fig. 5). Upon re-emission, they have relatively low energy and are already in regions where the plasma potential is near a maximum, giving them little opportunity to increase their energy substantially (beyond the 15 V sheath potential drop). Along the central axis and at axial locations downstream of the exit plane, the mean electron energy more closely tracks the plasma potential. In these regions, the electron population is dominated by plume-bound electrons which suffer fewer collisions (in some cases none), so the local mean electron energy is the initial energy plus the potential drop to the cathode.

We can estimate a random-walk diffusion coefficient, D, for those electrons which suffer a collision as $D=t_{\mathrm{coll}}V_z^2$, where t_{coll} is the mean time between collisions, and V_z is the mean axial velocity over each electron's lifetime. These estimates can be compared with the Bohm diffusion coefficient,[18] D_{Bohm}, which may be expressed as

$$D_{\mathrm{Bohm}} = \frac{\mathrm{k}T_{\mathrm{e}}}{16\mathrm{e}|\boldsymbol{B}|}, \tag{3}$$

where k is Boltzmann's constant, T_{e} is the electron temperature, e is the fundamental charge, and $|\boldsymbol{B}|$ is the magnitude of the magnetic field. In the near-field, D_{Bohm} varies considerably (given the variation in the electron temperature and magnetic field strength), but is of the order of 10^2 $\mathrm{m}^2\,\mathrm{s}^{-1}$ over the channel for the discharge studied. Measurements made on a similar thruster indicate that the axial cross-field diffusion coefficient in the near-field is in the range of $\sim 10^2$ to $\sim 10^4$ $\mathrm{m}^2\,\mathrm{s}^{-1}$.[26] In the nominal simulation, the mean random-walk diffusion coefficient (for those electrons which suffer collisions) is 2.2×10^3 $\mathrm{m}^2\,\mathrm{s}^{-1}$, about an order of magnitude greater than the Bohm prediction, but within the range of experimental values. The diffusion coefficient is elevated in part due to the existence of azimuthal components of $\boldsymbol{E}$ and $\boldsymbol{B}$, which combined with radial components of the fields cause electrons to drift axially (e.g., $E_\theta \times B_{\mathrm{r}}$ is in the $-z$ direction).

B. Sensitivity to cathode position

Due to the complex nature of the field distributions in the near-field (e.g., see Figs. 2 and 3), the initial cathode-born electron trajectories (and subsequent wall-collision locations) are strongly dependent on the cathode position. As a result, the fraction of electrons reaching the channel is expected to be sensitive to the cathode position.

A subset of simulations (each comprising 10^4 electrons) was executed in which the spatial position of the cathode was varied, but the other details of the electron launch were the same as in the previous section. Due to the computational cost of the simulations that implement a fluctuating plasma potential distribution, *static*, 3D electric and magnetic field distributions [as shown in Figs. 3(a) and 3(c)] were utilized in the sensitivity studies to allow more extensive investigation of the parameter space.

The cathode orientation was fixed at a pointing angle of 135° (see Fig. 1), approximately the experimental orientation. The divergence angle of the initial electron plume was set at 30°. The divergence angle is the solid angle (centered on the cathode centerline) within which one standard-deviation of the electrons are emitted, as in the previous study.[11]

The cathode position was varied over $0\ \mathrm{cm} \le r \le 16\ \mathrm{cm}$, $0\ \mathrm{cm} \le z \le 6\ \mathrm{cm}$, and $0° \le \theta \le 90°$. In each simulation, the fraction of electrons reaching the channel was calculated and is shown in Fig. 7. Areas which appear white in the figure are those in which <0.1% of the electrons reached the channel; about half of the studied cathode positions resulted in zero current reaching the channel.

Recent experimental studies have demonstrated that the cathode position[8] and electron emission details[27] strongly affect the thruster performance. The results of the simulations show that the fraction of electrons reaching the channel is strongly sensitive to the cathode position (Fig. 7), likely impacting thruster operation. In practice, the Hall discharge is tuned (by modulating the magnetic field) to maximize the ratio of the ion beam current to the discharge current, thus less electron current reaching the channel from the cathode may be desirable, provided sufficient electron current reaches the channel to sustain the discharge.

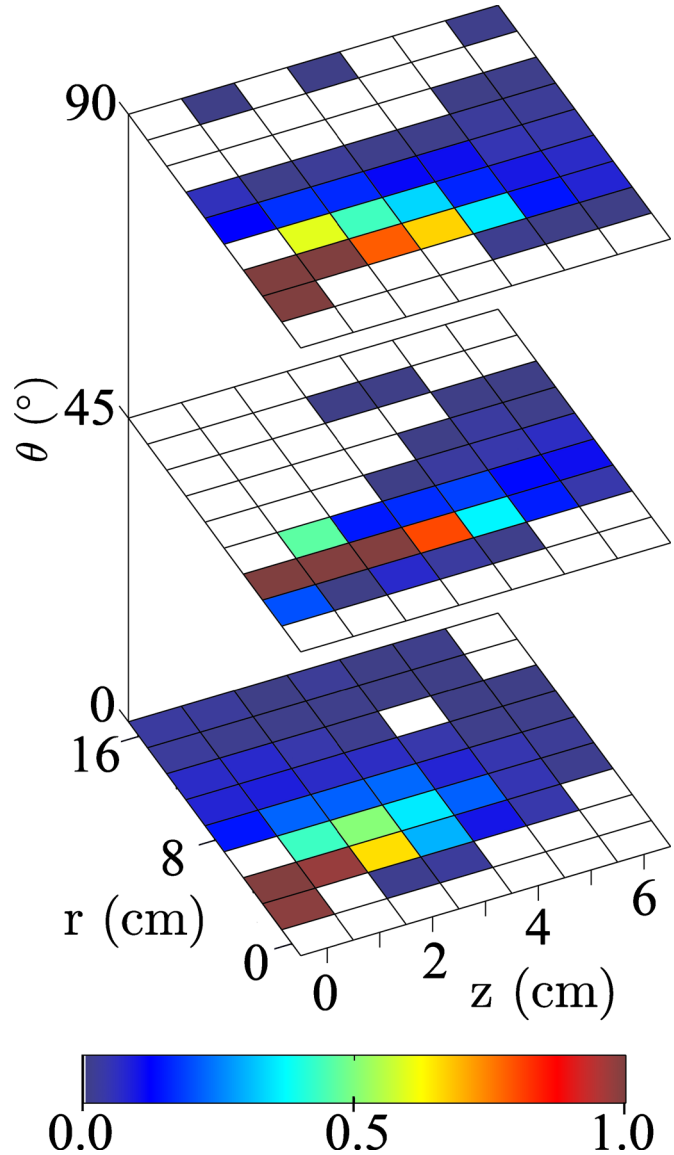

FIG. 7. (Color online) Simulated sensitivity of channel-bound electron fraction to cathode position.

The simulations suggest that there are several promising regions where the cathode may be placed. For instance, positioning the cathode at $[r,z,\theta]=[12\ \mathrm{cm}, 2\ \mathrm{cm}, 0°]$ (substantially away from the thruster plume) yielded a channel/beam current ratio of 7.1%; a relatively modest but perhaps sufficient amount of current to sustain the discharge. Positioning the cathode immediately downstream of the channel, i.e., near $r \approx 2$ to 4 cm and $z \approx 0$, resulted in the highest channel-current ratios. Some thruster designs, including the BHT-8000,[28] have a central cathode mounted within the thruster. When the cathode was positioned along the central axis (at $r=0$ cm) in the simulation, no electrons ever migrated to the channel, regardless of the axial position of the cathode. However, to model discharges with an internal cathode, the appropriate field structure must be implemented. In

the present thruster, the structure of the magnetic field along the central axis (the field lines are primarily axial) is conducive to electron current leaving the simulation domain in the plume. Furthermore, while the simulations suggest that zero electron current reaches the channel in many orientations where the experimental discharge might expect to be sustained, it is possible that fluctuations (such as those included in the nominal simulation), or interparticle collisions (discussed in a following subsection) are important for transporting electrons to the channel in these regions.

C. Sensitivity to cathode orientation and plume divergence

In addition to the spatial degrees of freedom already investigated, the cathode pointing angle can be varied, as can the divergence angle. While the divergence angle of the electron plume is typically not as easily controlled during thruster operation, modifications to the cathode design allow for this angle to be adjusted (e.g., an electron-emitting filament emits in all directions, whereas a typical hollow cathode emits electrons in a narrower beam). With this in mind, a second set of simulations was executed in which the cathode position was fixed at the nominal point, $[r,z,\theta]=[7.84\ \text{cm}, 2.2\ \text{cm}, 0°]$, but the pointing angle and divergence angle were varied; the other details of the electron launch were unchanged.

As in the previous sensitivity simulations (Sec. III B), static fields [shown in Figs. 3(a) and 3(c)] were implemented and 10^4 electrons were tracked throughout their lifetimes in each simulation. The pointing angle was varied from 0° (i.e., pointing along the $+y$-axis in Fig. 1) to 345° in 15° increments. Note that a pointing angle of 90° is along the $+z$-axis in Fig. 1. The divergence angle was varied from 0° to 180° in 15° increments.

Figure 8 shows the sensitivity of the fraction of electrons reaching the channel to the cathode pointing angle and divergence angle. As with the cathode position, the simulations are strongly sensitive to the cathode orientation. About 25% of the studied cathode orientations resulted in zero current reaching the channel. The greatest frequency of these events occurs when the cathode divergence is very narrow (i.e., the electrons leave the cathode in a focused beam). However, this narrow divergence also leads to the highest fraction of electrons reaching the channel for specific pointing angles. The cathode tip is positioned at $[r,z,\theta]=[7.84\ \text{cm}, 2.2\ \text{cm}, 0°]$ and the channel spans the radial coordinates of $r=2.08-3.66$ cm. Thus the pointing angles at which the cathode axis passes through the channel are from 191° to 208°. When the cathode pointing angle is 135° (see Fig. 1), the cathode is not pointing directly at the channel, but rather into the plume (a common orientation, in practice). Since the fraction of electrons reaching the channel is highly sensitive to the cathode orientation, tuning this parameter is expected to significantly affect performance. Furthermore, it appears that a more focused electron beam leaving the cathode increases the channel-bound current, perhaps undesirably.

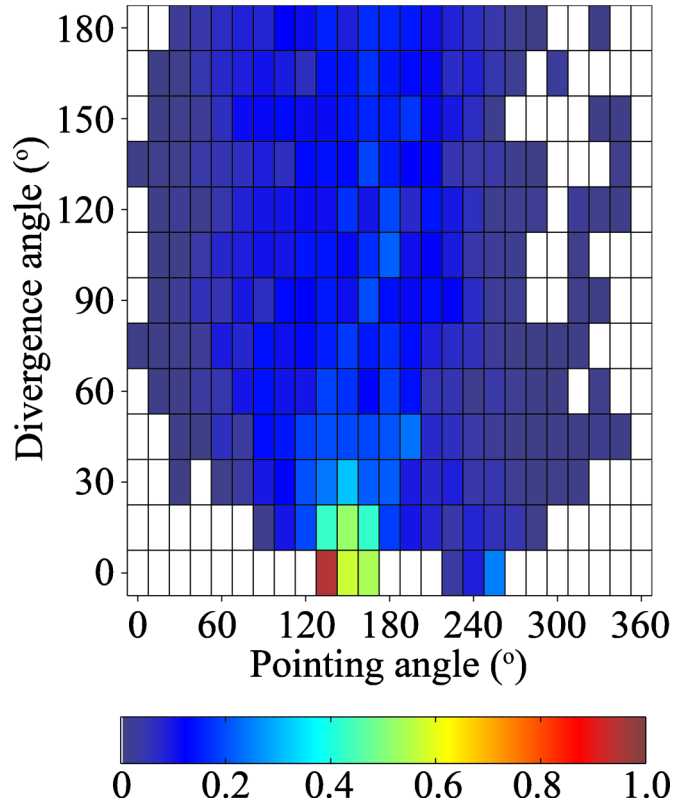

FIG. 8. (Color online) Simulated sensitivity of channel-bound electron fraction to cathode orientation and the initial electron beam divergence.

D. Influence of collisions

One important feature absent in the previous simulations was interparticle, gas-phase collisions. In reality, such collisions are occurring at a rate, ν_c, that is proportional to the number density of colliding species, n, the velocity of the species, v, and the velocity-dependent cross-section, $\sigma(v)$, i.e., $\nu_c \propto nv\sigma(v)$. This is a simplified expression which ignores the importance of the angle of incidence of the collisions as well as the velocity of the collision partner. The cross-section for momentum transfer of electrons in a Xe plasma is of the order of 10^{-20} to 10^{-19} m^2 for typical electron energies in the near-field (of the order of 3–30 eV).[29] Here we are neglecting the influence of ionization events and electron-ion collisions, though the effect of a greatly elevated collision rate is considered in the following section. Thus, in the regions of highest density in the near-field (where $n \sim 10^{18}$ m^{-3}),[30] the momentum-transfer collision frequency is approximately 3×10^5 s^{-1}. Each electron is expected to suffer a collision once every several microseconds in the densest regions of the near-field. Away from the exit plane (where the peak densities and energies are observed), the collision frequency drops rapidly.

In order to establish the effect that interparticle collisions may have on the electron transport in the near-field, a pair of simulations was executed in which gas-phase collisions were allowed to occur at a prescribed rate. The collision frequency was not spatially varied and electrons suffering a collision maintained their precollision energy with randomized velocity. The static, 3D fields shown in Figs. 3(a) and 3(b) were

prescribed and 10^5 electrons were launched and tracked throughout their lifetimes in each simulation.

In the first simulation, gas-phase collisions occurred randomly on average once every 10 μs, with a standard-deviation of 3 μs. This simulation is meant to approximate the collision frequency present at the exit plane. By applying this rate everywhere in the domain, the simulations results are intended to represent an upper limit on the effect of collisions. In the second simulation, gas-phase collisions occurred randomly on average once every 100 ns, with a standard-deviation of 30 ns; a rate more than two orders of magnitude higher than the peak rate expected. These simulations are meant to greatly exaggerate the effects of gas-phase collisions.

Neither rate had a significant effect on the channel to plume current ratio. At the expected collision rate (i.e., $\sim 10^5$ s^{-1}), the fraction of electrons reaching the channel (i.e., those which leave the domain at the channel boundary spanning $2.08 < r < 3.66$ cm at $z=0$) increasing by a very small margin from 34.73% in the static simulation without interparticle collisions to 35.13%. When interparticle collisions were introduced at the greatly exaggerated rate (i.e., $\sim 10^7$ s^{-1}), the fraction of electrons reaching the channel was only slightly lower, 31.0%.

The density of electrons remained very inhomogeneous, as Fig. 9 shows. In fact the simulated density for cases with interparticle collision rates of 10^5 s^{-1} [Fig. 9(d)] and 10^7 s^{-1} [Fig. 9(e)] was nearly identical to that observed in the static simulation without gas-phase collisions [see Fig. 9(b)]. These simulations suggest that gas-phase collisions, even at greatly exaggerated rates, have only a limited influence on the electron transport in the near-field.

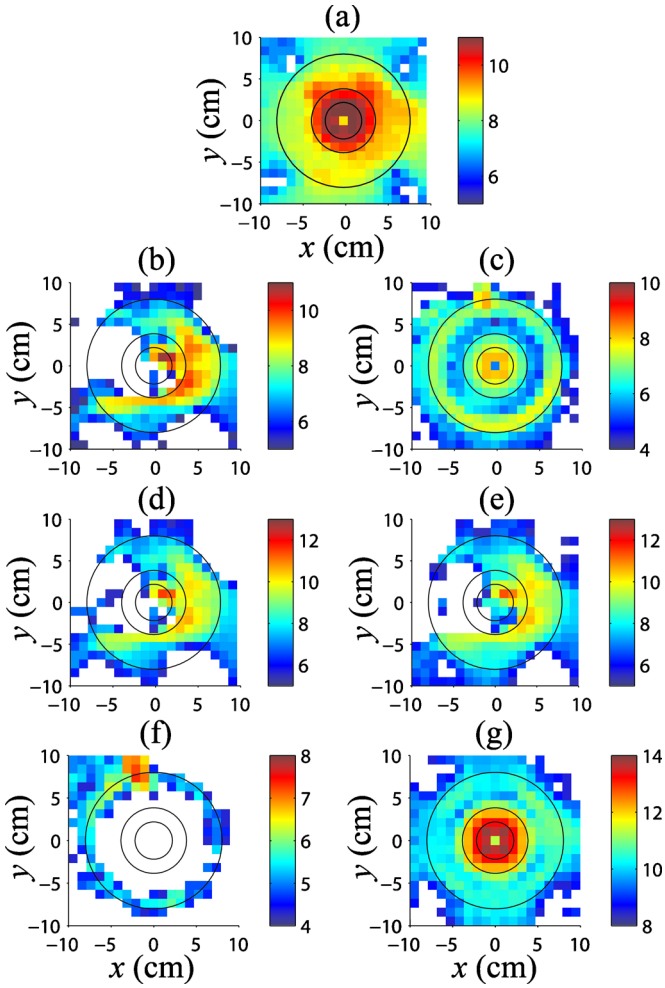

FIG. 9. (Color online) Electron density distribution (cm^{-3}, on a logarithmic scale) in the $z=0$ to 1 cm plane observed in the (a) nominal, (b) 3D static, (c) axisymmetric E and B, (d) $\nu_c = 10^5$ s^{-1}, (e) $\nu_c = 10^7$ s^{-1}, (f) axisymmetric B/3D E, and (g) axisymmetric E/3D B simulations. The channel and thruster boundaries are indicated by dark circles.

E. Influence of field symmetry

In the earlier study, the field distributions were estimated and assumed axisymmetric.[12] In the present work, the field distributions were inspired by more complete measurements that showed that the plasma potential was not axisymmetric. Furthermore, the discrete electromagnets present in the magnetic circuit often lead to azimuthal gradients in the magnetic field. A final subset of simulations was performed to gain insight into the role of $\boldsymbol{E}$ and $\boldsymbol{B}$ field symmetries. The fields were taken to be static in this study and one or both of $\boldsymbol{E}$ and $\boldsymbol{B}$ were prescribed to be axisymmetric (by azimuthally averaging the field distributions shown in Fig. 3). In each simulation, 10^5 electrons were launched.

When both fields were assumed axisymmetric, the electron density distribution was quite uniform azimuthally as shown in Fig. 9(c), but the lifetimes were much shorter, and the electron density was lower than that observed in the nominal 3D simulations with a helical plasma potential fluctuation [see Fig. 9(a)]. When only the magnetic field was prescribed to be axisymmetric, the density distribution was extremely inhomogeneous as shown in Fig. 9(f). In contrast, when only the electric field was prescribed to be axisymmetric, the density distribution much more closely resembled the nominal distribution [compare Figs. 9(a) and 9(g)].

Essentially no electron current reached the channel in the simulation that considered fully axisymmetric fields and in the simulation that considered only axisymmetric $\boldsymbol{B}$. By comparison, in the nominal simulation, 11.7% of the electrons reached the channel and 34.7% reached the channel in the static simulation that considered 3D fields. In the simulation that considered 3D $\boldsymbol{B}$ and axisymmetric $\boldsymbol{E}$, 15.5% of the electrons reached the channel. This result suggests that the three-dimensionality of the magnetic field is important to electron transport in the near-field. While the extent to which the magnetic field may be considered axisymmetric varies among various annular Hall thruster designs, the influence should not be overlooked in simulations.

IV. DISCUSSION

A series of simulations have been executed to evaluate the sensitivity of single-particle electron kinetic simulations of electron transport in the near-field of an annular Hall thruster to cathode position and orientation, interparticle collisions rates, and field symmetry. The overall results for many of the simulations are shown in Table I. In the table, the nominal simulation (with 3D fields and a 25 kHz helical

TABLE I. Summary of bulk simulation results including current distribution, mean lifetime, number of wall collisions (per electron), random-walk diffusion coefficients, and the velocity ratio, $|\beta^*|=|\overline{V_{\mathrm{E}\times\mathrm{B}}}/\overline{V_{\mathrm{E}}}|$.

Simulation	I_c/I_{tot}	τ ($\times 10^{-6}$ s) Tot	c	p	W Tot	c	p	D (m^2/s)	$\lvert\beta^*\rvert$
Nominal	0.113	1.88	6.55	1.28	6.85	32.7	3.55	2.2×10^3	0.02
3D, static	0.347	0.68	1.53	0.23	7.93	9.46	7.12	1.7×10^4	15.57
Axisymmetric	0.000	0.45	⋯	0.44	0.03	⋯	0.03	⋯	0.01
Expected ν_c	0.351	0.68	1.51	0.23	7.53	9.70	6.92	1.7×10^4	11.66
Exaggerated ν_c	0.310	0.62	1.39	0.28	7.06	7.52	5.88	1.3×10^4	5.91
3D $\boldsymbol{E}$	0.000	0.13	⋯	0.13	0.01	⋯	0.01	⋯	⋯
3D $\boldsymbol{B}$	0.155	34.0	47.2	29.3	50.6	76.2	42.2	1.4×10^3	0.14

plasma potential fluctuation) is referred to as the "nominal" simulation, while the analogous static simulation is referred to as "3D static." The simulation with axisymmetric fields is denoted "axisymmetric," and the simulations that implemented mixed axisymmetric/3D fields are denoted 3D $\boldsymbol{E}$ (axisymmetric $\boldsymbol{B}$-field) and 3D $\boldsymbol{B}$ (axisymmetric $\boldsymbol{E}$-field). The simulations that considered additional gas-phase collisions at expected (i.e., $\sim 10^5$ s^{-1}) and exaggerated (i.e., $\sim 10^7$ s^{-1}) rates are referred to as "expected ν_c" and "exaggerated ν_c," respectively. The fraction of electrons reaching the channel is denoted "I_c/I_{tot};" the labels "c," "p," and "tot" refer to the contribution from channel-bound, plume-bound, and the total population of electrons, respectively. The mean electron lifetime, τ, mean number of wall collisions suffered by each electron, W, and the estimated random-walk diffusion coefficient, D (calculated *only* for those electrons which suffer a collision in their lifetime) are also listed for comparison. Finally, the table lists another useful metric for quantifying the electron transport, the velocity ratio, $|\beta^*|=|\overline{V_{\mathrm{E}\times\mathrm{B}}}/\overline{V_{\mathrm{E}}}|$. The overbar indicates the average value of the electron population. In the table, $|\beta^*|$ is the azimuthally averaged value in the volume of space within the channel boundaries and 0 cm$<z\leq 1$ cm. Here, $\boldsymbol{E}$ and $\boldsymbol{B}$ are predominantly orthogonal and $|\beta^*|$ is an estimate of the inverse Hall parameter which may be compared with the $1/16\sim 0.06$ value predicted by Bohm diffusion.[18]

The addition of interparticle collisions had only a small impact on any of the results, even when these additional gas-phase collisions were prescribed to occur at rates about two orders of magnitude higher than expected in the plasmas of the Hall discharge studied in this work. The estimated inverse Hall parameter decreased in magnitude at the highest collision rates (by about 2/3) indicating that gas-phase collisions do enhance axial transport, but this is a modest reduction compared with the four orders of magnitude decrease observed in the nominal simulation. The current ratio fell by slightly more than 10% at the highest collision rates (likely due to a slight decrease in the number of wall-collision events) and the lifetimes and random-walk diffusion coefficients were all about the same as the analogous simulation without interparticle collisions (i.e., the 3D static simulation). While some gas-phase collisions will scatter electrons onto trajectories that are favorable to electron migration into the channel, some will be more favorable to electrons leaving in the plume. Electrons that were already diffusing toward the channel via near-wall transport may be scattered away, while others will be scattered toward the channel. The simulations suggest that these effects mostly cancel for the particular conditions studied herein. The density distributions were also essentially unchanged (see Fig. 9).

The simulation results demonstrate that the fraction of cathode electrons that reach the channel of the discharge is highly sensitive to the cathode position and orientation, as well as the divergence of the electron plume (e.g., see Figs. 7 and 8). Depending on the cathode location, as much as 100% of the electrons reach the channel, though many cathode locations result in zero electron current reaching the channel. Though the current simulation predicts zero electron current to the channel for internal cathode configurations (i.e., at $[r,z]=[0,0]$), the magnetic circuit in the current study does not consider the influence of the internal cathode. Furthermore, while gas-phase collisions were of little importance with external cathode configurations, it is possible that these events are important for internal cathode configurations

3D fields produce significantly different current ratios, lifetimes, and diffusion rates than axisymmetric fields or mixed fields (e.g., axisymmetric $\boldsymbol{E}$ and 3D $\boldsymbol{B}$). Helical plasma potential fluctuation (inspired by recent near-field experiments)[12] resulted in a significantly more homogenized electron density distribution and reduced electron current to the channel, compared with static fields. The random-walk diffusion coefficient in the 3D static simulation was 1.7×10^4 m^2 s^{-1}, but this value reduced to 2.2×10^3 m^2 s^{-1} in the nominal simulations, within the range of measurements,[26] but still about an order of magnitude greater than Bohm diffusion predicts. The decrease in the axial mobility (relative to the azimuthal mobility) occurs in tandem with the azimuthal homogenization of the electrons.

The estimated inverse Hall parameter, $|\beta^*|$, indicates that the helical waves in the nominal simulation greatly enhance the $\boldsymbol{E}\times\boldsymbol{B}$ drift velocity of the electrons, reducing the estimated inverse Hall parameter to 0.019; four orders of magnitude smaller than the 3D static result of 15.6, but only a few times smaller than the Bohm estimate of 0.06 (for electrons). The axisymmetric simulation also yielded a small es-

timated inverse Hall parameter; $|\beta^*|=0.014$, indicating that the electrons are largely confined in $\boldsymbol{E}\times\boldsymbol{B}$ drifts. The fraction of electrons reaching the channel was zero when axisymmetric fields were implemented, perhaps linked to the lack of wall-collision events which seem to play an important role in driving electron current to the channel. The density distribution in the axisymmetric simulation was azimuthally homogeneous, but the electron lifetimes were very short (450 ns compared to 1.88 μs in the nominal simulation), causing lower average densities than the simulations that considered 3D fields (see Fig. 9).

Mixed axisymmetric/3D fields lead to a sparse electron density distribution, zero electron current to the channel, extremely short lifetimes ($\sim$130 ns), and negligible wall-collision rates when the magnetic field was assumed axisymmetric. When the electric field was assumed axisymmetric (and $\boldsymbol{B}$ was considered in 3D), the results were exactly the opposite; a density distribution similar to the 3D, fluctuating simulation (despite the lack of fluctuations in the mixed-field-symmetry simulations), lifetimes exceeding 30 μs, and the highest average number of wall collisions per particle ($>$50).

In every simulation, channel-bound electrons suffer more collisions than plume-bound electrons (up to ten times as many in the nominal simulation). Furthermore, regions of elevated wall-collision flux and exit locations in the $z=0$ plane (see Fig. 5) tend to neighbor each other. Wall collisions and near-wall transport are key to electron-cross-field transport both toward the channel and onto trajectories that leave the domain. The nominal simulation resulted in lower electron current to the channel in part due to a redirection of wall collisions toward the central pole of the thruster (compared to the 3D static simulation) where the magnetic field distribution allows electrons to escape into the plume more readily.

Transport of cathode electrons in the near-field is strongly sensitive to cathode parameters including position, orientation, and cathode plume divergence. However, additional gas-phase collisions, even when considered at rates two orders of magnitude greater than predicted, had little impact on the bulk near-field electron transport.

In contrast, the results are strongly sensitive to the field symmetry. In simulations that considered axisymmetric fields, the electron current to the channel was reduced to zero, and electrons suffered few wall collisions. The results suggest that, in addition to near-wall transport along the front face of the thruster, 3D field effects are responsible for the observed rates of cross-field electron transport in the near-field of Hall thrusters. 3D fields with azimuthal components of $\boldsymbol{E}$ and $\boldsymbol{B}$, in tandem with radial field components enhance axial electron transport (e.g., $E_\theta\times B_r$ is in the $-z$ direction). Helical plasma potential waves inspired by those recently measured[12] reduced the electron transport to the channel and significantly homogenized the azimuthal distribution of electrons. The disparity between simulations that consider 3D or axisymmetric field distributions questions the ability of simulations that ignore the three-dimensionality of the near-field plasma

ACKNOWLEDGMENTS

Partial funding for A. W. Smith was received from the National Defense Science and Engineering Graduate Fellowship program. This research was supported by the Air Force Office of Scientific Research, with Dr. Mitat Birkan as program manager.

[1] W. Grossman, R. V. Hess, and H. A. Hassan, AIAA J. **6**, 1034 (1965).
[2] A. I. Morozov, A. Y. Kislov, and I. P. Zubkov, JETP Lett. **7**, 172 (1968).
[3] W. A. Hargus and M. A. Cappelli, Appl. Phys. B: Lasers Opt. **B72**, 961 (2001).
[4] J. A. Linnell and A. D. Gallimore, J. Propul. Power **22**, 1402 (2006).
[5] C. V. Young, M. A. Cappelli, and A. W. Smith, *Proceedings of the 31st International Electric Propulsion Conference*, Ann Arbor, MI, 2009 (Electric Rocket Propulsion Society, Fairview Park, OH, 2009), IEPC Paper No. 2009-166.
[6] Y. Raitses, A. Smirnov, and N. J. Fisch, Phys. Plasmas **16**, 057106 (2009).
[7] E. M. Granstedt, Y. Raitses, and N. J. Fisch, J. Appl. Phys. **104**, 103302 (2008).
[8] J. Sommerville and L. B. King, *Proceedings of the 30th International Electric Propulsion Conference*, Florence, Italy, 2007 (Electric Rocket Propulsion Society, Fairview Park, OH, 2007), IEPC Paper No. 2007-78.
[9] J. M. Fife, Ph.D. thesis, Massachusetts Institute of Technology, Cambridge, MA, 1998.
[10] G. J. M. Hagelaar, J. Bareilles, L. Garrigues, and J. P. Boeuf, J. Appl. Phys. **91**, 5592 (2002).
[11] A. W. Smith and M. A. Cappelli, J. Phys. D **43**, 045203 (2010).
[12] A. W. Smith and M. A. Cappelli, Phys. Plasmas **16**, 073504 (2009).
[13] M. K. Scharfe, N. Gascon, and M. A. Cappelli, Phys. Plasmas **13**, 083505 (2006).
[14] J. M. Fife, M. Martinez-Sanchez, and J. Szabo, *Proceedings of the 33rd AIAA/ASME/SAE/ASEE Joint Propulsion Conference and Exhibit*, Seattle, WA, 1997 (American Institute of Aeronautics and Astronautics, Reston VA, 1997), AIAA Paper No. 1997-3052.
[15] J. Bareilles, G. J. M. Hagelaar, L. Garrigues, C. Boniface, J. P. Boeuf, and N. Gascon, Phys. Plasmas **11**, 3035 (2004).
[16] E. Fernandez, M. A. Cappelli, K. Mahesh, Center for Turbulence Research Annual Research Briefs, Stanford University, 1998, p. 81.
[17] E. Fernandez, A. Knoll, and M. Cappelli, *Proceedings of the 29th International Electric Propulsion Conference*, Princeton, NJ, 2005 (Electric Rocket Propulsion Society, Fairview Park, OH, 2005), IEPC Paper No. 2005-197.
[18] D. Bohm, H. S. Burhop, and H. S. W. Massey, in *The Characteristics of Electrical Discharges in Magnetic Fields*, edited by A. Guthrie and R. K. Wakerling (McGraw Hill, New York, 1949).
[19] S. Yoshikawa and D. J. Rose, Phys. Fluids **5**, 3 (1962).
[20] J. A. Bittencourt, *Fundamentals of Plasma Physics*, 3rd ed. (Springer, New York, 2004), p. 282.
[21] C. A. Thomas, N. Gascon, and M. A. Cappelli, Phys. Rev. E **74**, 056402 (2006).
[22] D. Meeker, Finite Element Method Magnetics, version 4.0, software package, 2004.
[23] P. Moin, *Fundamentals of Engineering Numerical Analysis* (Cambridge University Press, Cambridge, 2001), p. 62.
[24] A. I. Morozov and V. V. Savel'ev, Plasma Phys. Rep. **27**, 570 (2001).
[25] M. A. Cappelli, N. Gascon, and W. A. Hargus, Jr., J. Phys. D **39**, 4582 (2006).
[26] N. B. Meezan, W. A. Hargus, Jr., and M. A. Cappelli, Phys. Rev. E **63**, 026410 (2001).
[27] Y. Raitses, E. Granstedt, A. Smirnov, E. Merino, and N. J. Fisch, *Proceedings of the 44th AIAA/ASME/SAE/ASEE Joint Propulsion Conference and Exhibit*, Hartford, CT, 2008 (American Institute of Aeronautics and Astronautics, Reston, VA, 2008), AIAA Paper No. 2008-5188.
[28] R. R. Hofer, L. K. Johnson, D. M. Goebel, and D. J. Fitzgerald, *Proceedings of the 42nd AIAA/ASME/SAE/ASEE Joint Propulsion Conference and Exhibit*, Sacramento, CA, 2006 (American Institute of Aeronautics and Astronautics, Reston, VA, 2006), AIAA Paper No. 2006-4482.
[29] W. L. Morgan, J. P. Boeuf, and L. C. Pitchford, Siglo-Kinema electron-molecule cross-sections, Kinema Research and Software, Monument, CO, software package, 1998, http://www.siglo-kinema.com.
[30] I. D. Boyd and R. A. Dressler, J. Appl. Phys. **92**, 1764 (2002).